NEUROSCIENCE

Directed and acyclic synaptic connectivity in the human layer 2-3 cortical microcircuit

Yangfan Peng[1]*†, Antje Bjelde[1], Pau Vilimelis Aceituno[2], Franz X. Mittermaier[1], Henrike Planert[1], Sabine Grosser[3], Julia Onken[4], Katharina Faust[4], Thilo Kalbhenn[5], Matthias Simon[5], Helena Radbruch[6], Pawel Fidzinski[7,8], Dietmar Schmitz[8,9], Henrik Alle[1], Martin Holtkamp[10], Imre Vida[3], Benjamin F. Grewe[2], Jörg R. P. Geiger[1]*

The computational capabilities of neuronal networks are fundamentally constrained by their specific connectivity. Previous studies of cortical connectivity have mostly been carried out in rodents; whether the principles established therein also apply to the evolutionarily expanded human cortex is unclear. We studied network properties within the human temporal cortex using samples obtained from brain surgery. We analyzed multineuron patch-clamp recordings in layer 2-3 pyramidal neurons and identified substantial differences compared with rodents. Reciprocity showed random distribution, synaptic strength was independent from connection probability, and connectivity of the supragranular temporal cortex followed a directed and mostly acyclic graph topology. Application of these principles in neuronal models increased dimensionality of network dynamics, suggesting a critical role for cortical computation.

Information in the brain is processed by interacting neurons whose activity is shaped by synaptic connectivity (*1*, *2*). Local synapses in rodent brains form recurrent networks with nonrandom structures, which have been implicated in various computations (*3*–*6*), such as pattern completion or directional tuning (*7*, *8*). These local and intralaminar excitatory synapses between cortical pyramidal neurons are mediated through basal dendrites and have been attributed to bottom-up information processing (*9*). How these rodent microcircuit principles and their computational implications translate to the evolutionarily expanded layer 2-3 (L2-3) of the human neocortex is unresolved. Studies of the human cortex have uncovered a higher complexity at the cellular level (*10*–*19*), which implies distinct microcircuit architectures underlying superior cognitive abilities of humans (*20*). In this study, we tested whether the connectivity structure within L2-3 of the human cortex also exhibits adaptation for increased representational capacity and dimensionality (*21*, *22*). We analyzed a dataset on monosynaptic connections identified by multineuron patch-clamp recordings from acute human cortical brain slices (*15*, *23*). The tissue was obtained from anterior temporal lobectomies performed on temporal lobe epilepsy (TLE) patients (n = 23). By recording up to 150 monosynaptic connections per cortical sample, we were able to derive essential wiring principles of the human cortical microcircuit. We further modeled and simulated these principles in recurrent neural networks and identified how they affect the dimensionality of neural activity and computation.

[1]Institute of Neurophysiology, Charité–Universitätsmedizin Berlin, corporate member of Freie Universität Berlin and Humboldt Universität zu Berlin, 10117 Berlin, Germany. [2]Institute of Neuroinformatics, University of Zurich and ETH Zurich, 8057 Zürich, Switzerland. [3]Institute for Integrative Neuroanatomy, Charité–Universitätsmedizin Berlin, corporate member of Freie Universität Berlin and Humboldt Universität zu Berlin, 10117 Berlin, Germany. [4]Department of Neurosurgery, Charité–Universitätsmedizin Berlin, corporate member of Freie Universität Berlin and Humboldt Universität zu Berlin, 10117 Berlin, Germany. [5]Department of Neurosurgery (Evangelisches Klinikum Bethel), Medical School, Bielefeld University, 33617 Bielefeld, Germany. [6]Department of Neuropathology, Charité–Universitätsmedizin Berlin, corporate member of Freie Universität Berlin and Humboldt Universität zu Berlin, 10117 Berlin, Germany. [7]Clinical Study Center, Berlin Institute of Health at Charité–Universitätsmedizin Berlin, 10117 Berlin, Germany. [8]German Center for Neurodegenerative Diseases (DZNE) Berlin, 10117 Berlin, Germany. [9]Neuroscience Research Center, Charité–Universitätsmedizin Berlin, corporate member of Freie Universität Berlin and Humboldt Universität zu Berlin, 10117 Berlin, Germany. [10]Epilepsy-Center Berlin-Brandenburg, Department of Neurology, Charité–Universitätsmedizin Berlin, corporate member of Freie Universität Berlin and Humboldt Universität zu Berlin, 10117 Berlin, Germany.
***Corresponding author. Email: yangfan.peng@charite.de (Y.P.); joerg.geiger@charite.de (J.R.P.G.)**
†Present address: Department of Neurology and Neuroscience Research Center, Charité–Universitätsmedizin Berlin, 10117 Berlin, Germany.

Local connectivity is heterogeneously distributed

To analyze the network architecture of the human neocortex, we made use of our previously reported dataset on cellular and synaptic properties of L2-3 pyramidal cells (PCs) from the temporal cortex of TLE patients (Fig. 1A; see methods in the supplementary materials) (*15*) and focused on the connectivity patterns. A hallmark feature in rodent cortical network topology is the overrepresentation of reciprocal connections compared with Erdős-Rényi (ER) random network models (*4*, *5*, *24*–*27*). ER models are random graphs wherein each directed connection between two nodes is independently established with a uniform probability. In our study, this means that connections are simulated based on the pooled connection probability that is determined by the ratio of all observed to all tested connections. In our human data from TLE patients, we found no overrepresentation of reciprocity, as we obse only 96 reciprocal pairs out of 3600 te pairs. This is in good agreement with a generic ER model (90 ± 10, mean ± SD) for random connectivity at the observed pooled connection probability of 15.8% (1137 out of 7200 tested connections; Fig. 1B; see methods). However, pooling connections across different recordings could potentially obscure relevant structure in the connectivity.

To address this limitation, we analyzed the connectivity at the level of independent multineuron patch-clamp recordings. In each recording, we probed all possible connections between neurons recorded at the same time, referring to this group as a "cluster." By recording up to 10 neurons in one cluster (cluster size = 10), we probed up to 90 potential synaptic connections at once (*23*). Our cluster-level analysis showed consistent unidirectional (16.4 ± 10.6%, mean ± SD) and reciprocal connectivity (2.7 ± 5.3%), regardless of cluster size (Fig. 1C). Despite this consistency in mean connectivity, we found substantial variability between clusters, with connection probabilities ranging from 0 to 50%, even within the same tissue sample (fig. S1). We quantified this cluster variability using the coefficient of variance (CV), which also remained high in larger clusters of 6 to 10 neurons (0.4 to 0.6; fig. S2A). In this range, cluster variability was also independent of patient-specific sampling differences (fig. S2B). Finally, cluster variability was preserved when controlling for slicing angle and cut axons (fig. S2, C and D). Specifically, in our analysis of 787 pyramidal neurons with morphologically confirmed intact axons, we found that 30 to 40% of these neurons had no out-connections, even in neurons with a high number of tested connections (fig. S2E). This skewed distribution of out-degrees of individual neurons forms the basis for the heterogeneous distribution of cluster connectivity, indicating that low connectivity in clusters can arise irrespective of axon cutting or sampling strategy.

Reciprocal connectivity is random and not stronger

To assess the contribution of this nonrandom connectivity to the predicted reciprocity, we generated a model accounting for cluster-specific connection probabilities (see methods). This "heterogeneous cluster Erdős-Rényi model" (het-ER) predicted an even slightly higher reciprocal connectivity compared with the pooled data (117 ± 10 versus 96; Fig. 1, B and C). Furthermore, reciprocal connectivity on the cluster level was, on average, similar to or lower than that predicted by the het-ER model across clusters with different connection probabilities (fig. S3A). This suggests that there is no overrepresentation of reciprocity in the temporal cortex beyond the identified heterogeneous cluster connectivity. To further analyze this

clustered network topology, we counted the number of common (synaptically connected) neighbors for each probed neuron pair (see methods). In line with previous reports (*5*), pairs with more common neighbors had higher connection probabilities. However, the same trend was also present in simulations of the het-ER model (Fig. 1D). These results were also evident when analyzed on the patient level (fig. S3B). Thus, the common-neighbor rule does not represent a major wiring principle beyond the identified heterogeneously distributed connectivity.

Another hallmark of rodent cortical microcircuit studies is the increased excitatory postsynaptic potentials (EPSPs) in reciprocal pairs and densely connected clusters (*4*, *5*, *27*). In line with previous synaptic connectivity studies, we found lognormal EPSP amplitude distributions (lognormal fit estimates: $\mu = -0.91$, $\sigma = 1.02$). However, in our human data, EPSP amplitude of reciprocal connections was not statistically different compared with unidirectional connections (0.38 versus 0.43 mV, $P = 0.05$, Mann-Whitney U test; Fig. 1E). EPSP amplitudes also showed no significant relationship to cluster connectivity ($P = 0.55$, linear mixed effect model; Fig. 1E) or number of common neighbors ($P = 0.42$, one-way analysis of variance; Fig. 1D). The independence of EPSP amplitude from local connectivity was further preserved across different cluster sizes and at the patient level (fig. S3, C to E). These differences in comparison to juvenile rodent cortices could arise through age, region, and species specificity.

Local connectivity is directed

In cortical microcircuits, higher-order network motifs have been studied, revealing nonrandom features of synaptic connectivity (*4*, *28*, *29*). One common approach to study network structure beyond pairwise statistics is to consider triadic motifs, which describe the 16 nonisomorphic configurations of how three nodes can be interconnected (*28*). We found the profile of over- and underrepresentation of triadic motifs, relative to the ER model, to be similar to that in rodents (Fig. 1F; see methods) (*4*, *6*, *30*). However, the het-ER model, which accounts for the highly variable distribution of connectivity, was able to substantially reduce the number of nonrandom motifs, in line with theoretical predictions and connectivity data from electron microscopy (*25*, *29*). The overrepresentation of the directed and marked underrepresentation of the cyclic triadic motif remained unexplained. Directed transitive motifs and simplices have been previously identified as relevant network structures (*31*). We thus analyzed directed and simplicial motifs of higher order and found them to be consistently overrepresented compared with ER and not completely approximated by the

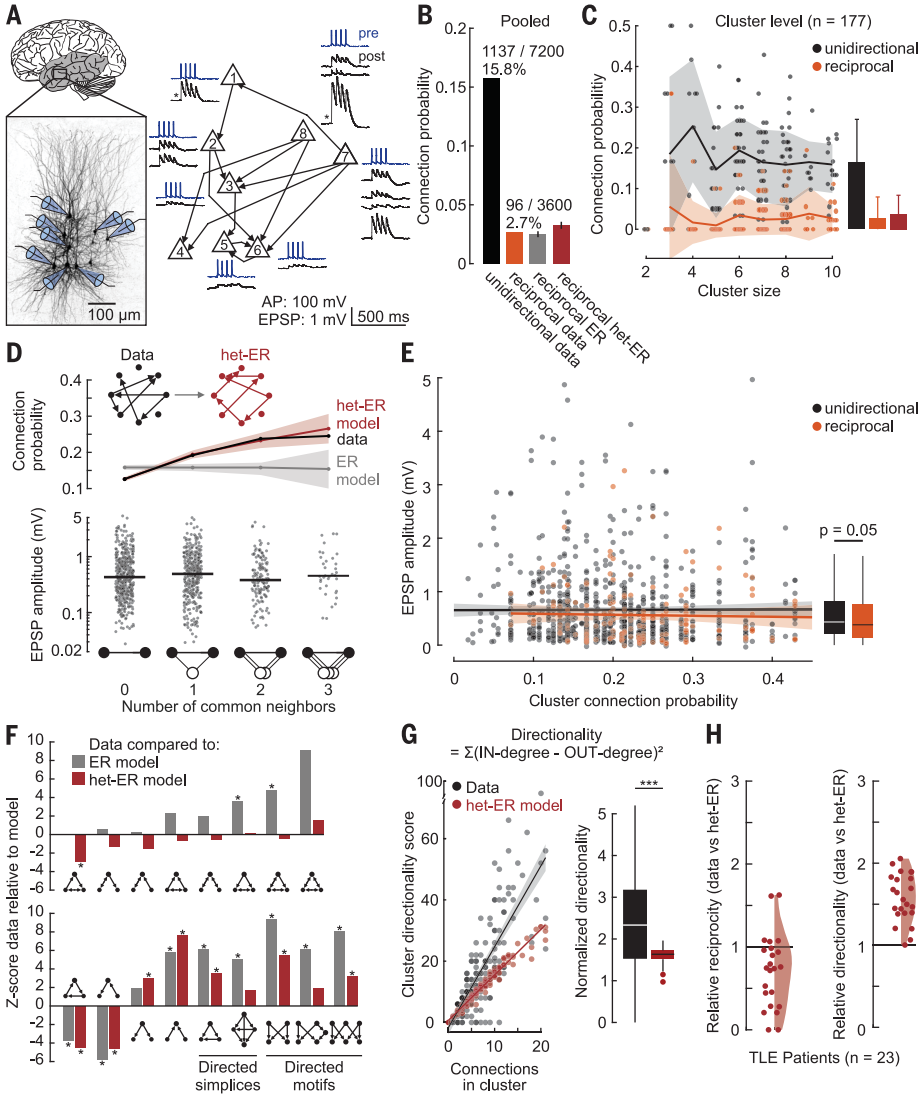

Fig. 1. Connectivity and synaptic strength in the human cortical microcircuit. (**A**) Multineuron patch-clamp recordings from one example cluster with eight L2-3 pyramidal neurons in human middle temporal gyrus. Graph depicts monosynaptic connections between neurons at spatial locations. Current-clamp traces show elicited action potentials (APs) of presynaptic neurons (black) above EPSPs of connected postsynaptic neurons (blue). Asterisks mark traces that have been scaled down by a factor of two. (**B**) Probabilities of unidirectional (black) and reciprocal (orange) connections. Gray and red represent expected reciprocity based on random models. Error bars indicate standard deviation in models. (**C**) Scatter plot of unidirectional and reciprocal connection probability of each cluster ($n = 177$) for different cluster sizes (number of neurons in cluster). Bar plots show probability of recorded clusters (black, orange) and simulated clusters (red: het-ER). Line and bars represent means, shade and error bars represent standard deviation. (**D**) (Top) Connection probability (lines) of pairs (filled circles) with different numbers of common neighbors (open circles) in data (black) and in random models (gray, red). Shaded areas represent bootstrapped 95% confidence intervals. (Bottom) EPSP amplitude distributions (log scale) are shown for pairs with different numbers of common neighbors. Horizontal lines indicate the median. (**E**) EPSP amplitudes of monosynaptic connections (dots) shown for different connection probabilities of the cluster from which each connection was recorded, colored by unidirectional (black) or reciprocal (orange) connection. Lines represent linear fits. Box plots on the right show pooled data. P value calculated by Mann-Whitney U test. (**F**) Normalized over- or underrepresentation of different network motifs in the data compared with random models (gray, red). Asterisks mark statistically significant deviations from the random model, corresponding to z-scores exceeding 2.3. This threshold represents an adjusted significance level ($\alpha = 0.05$), calculated using the false discovery rate. (**G**) Directionality score for each cluster ($n = 177$) dependent on its number of connections based on data (black) and the het-ER model (red). Lines represent linear fits. Box plot shows directionality of clusters divided by the number of connections. ***$P < 0.001$, paired t test. (**H**) Scatter points represent cumulative reciprocity and directionality calculated for each patient, divided by the het-ER model prediction. Shaded curves represent fitted kernel distributions.

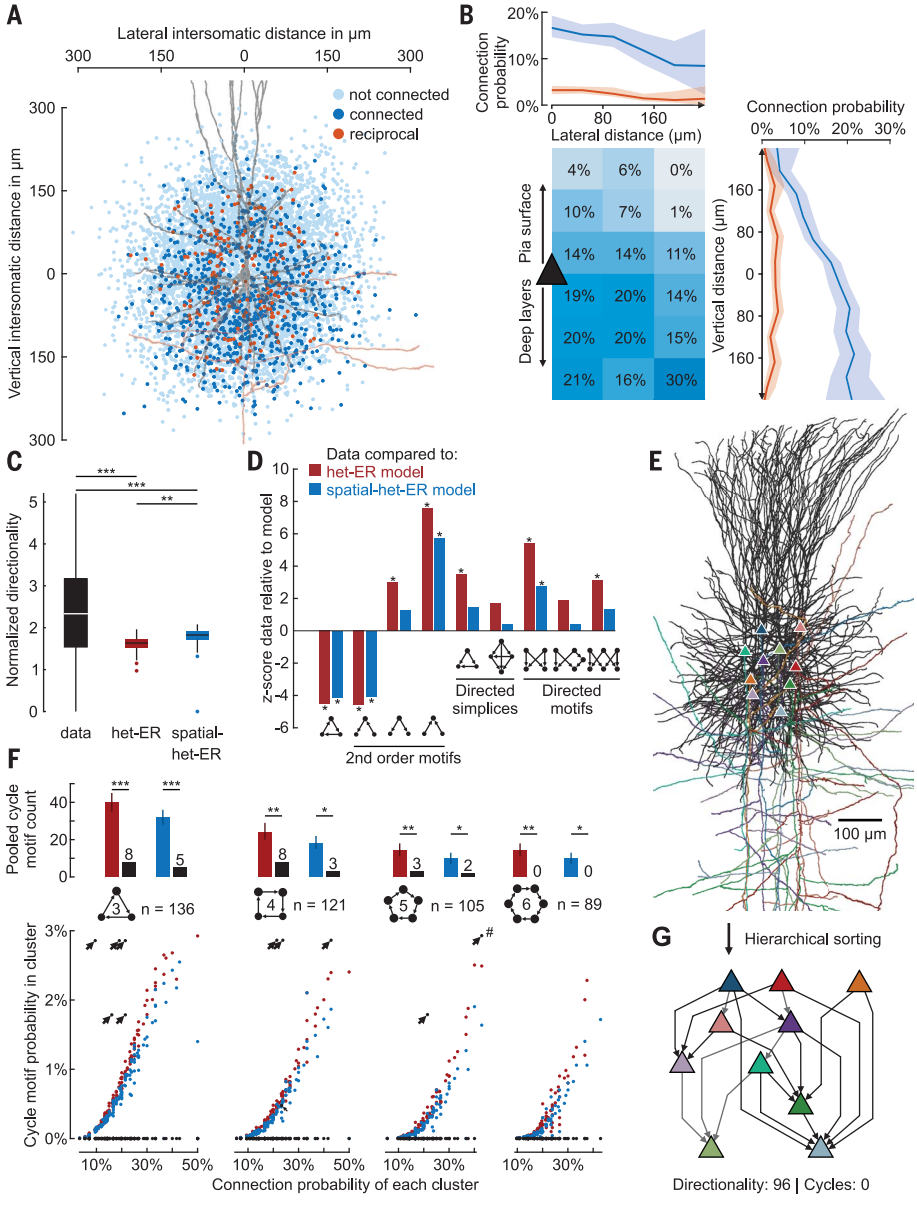

Fig. 2. Spatially biased connectivity and lack of cycles. (**A**) Probed (light blue), identified (dark blue), and reciprocal (orange) connections (dots) at relative lateral and vertical intersomatic distances, with the presynaptic soma aligned to origin, represented by example neuron reconstruction with axon in red. (**B**) Connection probability for 80 µm by 80 µm bins around the presynaptic soma, pooling data from lateral sides. Line plots show increasing connectivity toward deeper neurons and a lateral drop in connectivity: blue for unidirectional, orange for reciprocal connectivity. Shaded areas represent boot-strapped 95% confidence intervals. (**C**) Box plots represent the normalized directionality (divided by number of connections) of all recorded (black) and simulated clusters (red, blue). ***$P < 0.001$, **$P < 0.01$, paired t test. (**D**) Normalized relative over- and underrepresentation of selected motifs from Fig. 1F compared with random models (red, blue). Spatial-het-ER model only includes clusters with available neuron location. Asterisks mark statistically significant deviations from the random model, corresponding to z-scores exceeding 2.3. This threshold represents an adjusted significance level ($\alpha = 0.05$), calculated using the false discovery rate. (**E**) Reconstruction of the cluster with highest directionality score. Colored triangles represent soma locations, axons are colored for each neuron, and all dendrites are black. (**F**) (Top) Total motif count of cyclic motifs in the data (black bars) compared with the median count in the random model simulations (colored bars). Note that for comparison with spatial models (blue bars), neurons without coordinates were excluded. Error bars represent the interquartile range. P values from rank-based statistical test: ***$P < 0.001$, **$P < 0.01$, *$P < 0.05$. (Bottom) Observed (black) and simulated (red, blue) mean probability of different cyclic motifs for each cluster (dots). Clusters without spatial coordinates are not shown. Arrows highlight clusters with nonzero cycle probability. The recorded cluster marked with a hashtag has a cycle motif probability of 4.8% and has been moved for visualization. (**G**) Hierarchically sorted monosynaptic connectivity graph of cluster from (E). Colored triangles indicate same neurons as in (E). Fourteen connections target deeper neurons (black arrows), and six connections target more superficial neurons (gray arrows).

het-ER model (Fig. 1F; see methods). Similar results were also present at the patient level and when only including larger clusters (fig. S4, A and B). These results suggest that the network exhibits directed structures that cannot be explained by the nonrandom distribution of cluster connectivity. To establish a general measure of directionality at the cluster level, we calculated a directionality score for each cluster. This measure estimates the "feed-forwardness" of a given network on the basis of the cumulative difference between in- and out-connections of each neuron (*31*) (Fig. 1G; see methods). Directionality in the data was significantly higher than predicted by the het-ER model (2.5 ± 1.1 versus 1.6 ± 0.2, mean ± SD of normalized directionality, $P < 0.001$, paired t test), especially in densely connected clusters (Fig. 1G).

Directionality is independent of epilepsy factors

This study was performed on cortical tissue of individuals with drug-resistant TLE. To extend our findings to patients without TLE, we obtained tissue across different cortical areas from tumor surgeries of individuals with (n = 5) and without symptomatic epilepsy (n = 4; fig. S5). Connection probability between L2-3 PCs in tissue from individuals with tumors was lower than in tissue from individuals with TLE (9%, 165/1916, P = 0.001, Mann Whitney U test at patient level; fig. S5B). Median synaptic amplitudes were slightly lower (0.38 versus 0.45 mV, P = 0.02), but the overall distribution was very similar (interquartile range: 0.61 versus 0.62 mV; fig. S5C). To estimate the impact at the level of single individuals, we computed individualized estimates of reciprocity and directionality. These cumulative measures are robust proxies for network recurrency that can be compared with the het-ER model (see methods). Reciprocity and directionality were more heterogeneous in individuals with tumors than in those with TLE (fig. S5D), possibly because of additional confounds such as different brain regions, age range, tumor entity, and presurgical tumor treatment. A subset of

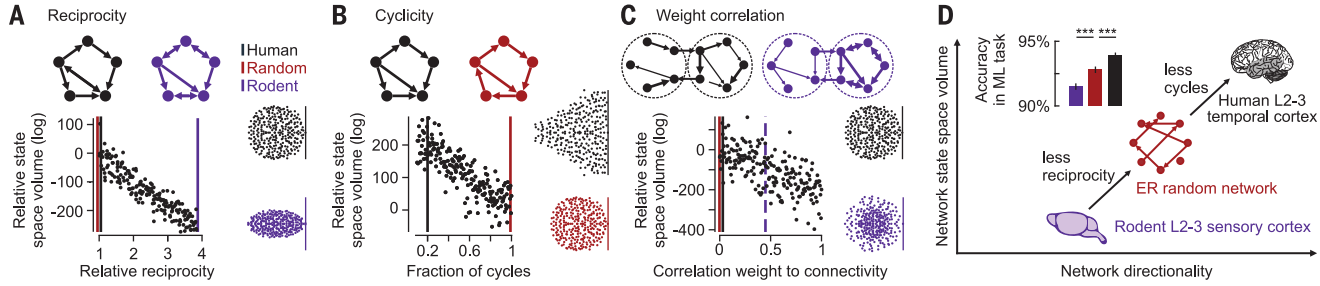

Fig. 3. Impact of network principles of the human L2-3 temporal cortex on network dimensionality. (**A** to **C**) For different network principles, the top graph illustrates the network structure found in humans (black), ER random model (red), and rodents (purple). The scatter plots show the state space volume of simulated networks with different degrees of reciprocity, weight correlation, or cyclicity, relative to the state space volume of a random ER network. The scattered schematic to the right shows the distribution of eigenvalues of the effective connectivity between the pyramidal neurons. Note that the weights in all simulations are scaled to maintain the maximum real part of the eigenvalues at one (vertical line) to ensure that the network remains at the edge of stability (see methods). (**D**) Schematic representation of the relationship between the directionality of a network (increased by reduced reciprocity and cyclicity) and the network state space volume. Bar graph shows the performance in a speech recognition [machine learning (ML)] task of simulated networks that are constrained by rodent-like higher reciprocity (purple), ER random connectivity (red), and human temporal cortex–like acyclicity (black) (see supplementary text section 2.3). Bars represent mean and SD from 100 simulations. The rodent L2-3 sensory cortex has lower network directionality, which corresponds to lower network state space. The human L2-3 temporal cortex exhibits an increased network directionality through lower reciprocity and cyclicity, which leads to a higher network state space volume.

individuals with tumors, with and without symptomatic epileptic seizures, exhibited microcircuit principles that resemble our epilepsy data, such as underrepresentation of reciprocity and increased directionality (fig. S5, A and D). Those cases suggest that these network properties are not specific to the temporal cortex or the TLE condition. However, to what extent other cortical regions resemble our results remains to be established. We next aimed to estimate the impact of epilepsy-associated confounds within our TLE cohort, which exhibited varying clinical phenotypes (ranging from 2 to 50 years disease duration and 2 to 30 seizures per month). Our individual-level analysis showed random or underrepresentation of reciprocity and increased directionality consistently across individuals and irrespective of hemisphere, sex, pathology, disease duration, seizure frequency, and medication intake (Fig. 1H and fig. S6). The fact that we observed these properties across individuals despite substantial differences in disease phenotype suggests that epilepsy-associated alterations are not major contributors to the identified microcircuit principles.

Vertical connectivity is spatially directed

Our results indicate that the observed networks are more directional than the het-ER model, suggesting additional nonrandom structures. One well-known constraint on connectivity is the relative anatomical location of the neurons. We reconstructed spatial offsets of neuron pairs based on the postsynaptic and presynaptic soma location (Fig. 2A). Consistent with rodent studies (*4*) and as reported in our previous study on this dataset (*15*), connection probability decreased with increasing intersomatic distance. Given the large sample size in our data, we were able to quantify the interaction of both distance and direction by distinguishing intersomatic distances along the vertical and lateral axes (Fig. 2B). We found that connection probability decreased with increasing lateral distance and toward the apical dendrite. Contrary to the expected distance-dependent decrease of connectivity, the connection probability increased when the postsynaptic soma was located at deeper positions along the vertical axis (Fig. 2B). This was observed irrespective of laminar depth and across individual subjects ($P < 0.001$, linear mixed effect model; fig. S7). As direction-dependent connection probability has also been found in rodents (*5*), we propose that this spatially directed connectivity represents a principle that is shared across species.

To determine whether this asymmetry could account for the network motifs and directionality, we generated a "spatial heterogeneous ER" model (spatial-het-ER) that incorporates the anatomically biased connectivity and the heterogeneous cluster connectivity (see methods). We found that this combined spatial-het-ER model had a significantly higher directionality at the cluster level than did the het-ER model (median: 1.8 versus 1.6, $P < 0.001$, Mann-Whitney U test) but did not explain the full extent of directionality in the data (median: 2.3; Fig. 2C). To further disentangle the unexplained directionality, we assessed the spatial-het-ER model prediction for a subset of the previously overrepresented motifs. We found that the spatial model was able to reduce the overrepresentation of these directed motifs by >50% compared with the het-ER model (Fig. 2D and fig. S4). This suggests that the spatially asymmetric connectivity contributes strongly to the directed network topology. However, the model still leaves a substantial residual directionality unexplained, indicating a feed-forwardness in the network beyond spatial asymmetry. The residual directionality could arise from the fact that neither the het-ER model nor the spatial-het-ER model is able to account for the underrepresentation of cyclic triadic motifs (Fig. 2D). As cycles increase the number of overall connections with zero contribution to the directionality score (see methods), the increased normalized directionality in the data could result from a more general underrepresentation of cyclicity in the clusters.

Local connectivity is largely acyclic

Thus, we investigated cyclic motifs with four, five, and six neurons that are connected in such a way that they form a unidirectional cycle and found a similar underrepresentation (see methods). The pooled number of these cyclic motifs in all recorded clusters was underrepresented compared with the model predictions (Fig. 2F, top row). To confirm the underrepresentation of cyclic motifs at the level of independently recorded clusters, we analyzed the frequency of cycles of different lengths in each cluster. We found that most clusters—and especially the densely connected ones—do not exhibit any cyclic motifs, whereas the het-ER and spatial-het-ER models predict an increase of cyclic motifs with increasing connectivity (Fig. 2F, bottom row). Although the sampled cluster sizes limit investigation of even bigger cycles, our ability to sort recorded clusters with dense connectivity as fully hierarchical graphs highlights the directed and acyclic structure of intralaminar network topology within the human L2-3 temporal cortex (Fig. 2, E and G).

Identified network principles increase computational capacity

To explore the implications of the network features identified in the human L2-3 microcircuit on neural activity, we simulated neural network

models based on the empirically identified connection probabilities, including the connectivity between pyramidal neurons and interneurons (PC-IN: 24.5%, 53/216; IN-PC: 25%, 54/216; fig. S8; see methods). We adapted the model network directionality by varying reciprocity and fraction of short cycles (Fig. 3C, A and B). We further constrained the models by varying the correlation between connection probability and strength (Fig. 3C; see methods). To have networks that are comparable in terms of dynamics, we kept the excitation/inhibition balance and scaled the weights to maintain the network at the edge of stability or at criticality (*32*). This means that networks with lower reciprocity or cyclicity have stronger weights (see supplementary text section 1.3). Following previous works on recurrent neural networks and random matrix theory (*33*), we studied the effects of our identified network principles on the activity in network models both analytically (supplementary text section 1) and in simulation (see methods). Specifically, we focused on the variability and independence of neuron population activity and formalized this using a metric describing the neural state space volume (supplementary text section 1). Rodent-like networks with a higher reciprocity have a smaller state space volume than do random and humanlike networks (Fig. 3A); this is because eigenvalues of the effective connectivity matrix are less spread out on the imaginary plane (Fig. 3A; supplementary text section 1). We further found that the removal of short cycles also increased the state space volume of the network (Fig. 3B). Finally, to assess how correlation between connection probability and strength affects network activity, we created two clusters with different connectivity and distributed the weights independently or in accordance with connection probability. High correlation of probability and weight, as has been attributed to the rodent sensory cortex (*27*), leads to a smaller state space volume in the network activity and a more contracted distribution of eigenvalues (Fig. 3C). These relationships between state space volume and the network principles remained unchanged when constrained by the connectivity and weights observed in the tumor cohort (fig. S5D; supplementary text section 1.4).

To study the computational implication of the increased state space volume, we trained recurrent neural networks with these principles on several machine learning tasks (supplementary text section 2). On a task that requires long memory and rich features (spoken digit recognition; supplementary text section 2.2), we found that networks with high reciprocity (rodent-like) had lower task performance compared with an ER network (91.5% versus 92.8%, mean accuracy of 200-neuron networks, $P < 0.001$; Fig. 3D). Furthermore, equally large networks with fewer short cycles (human temporal cortex–like) had a higher task performance compared with ER networks (93.9% versus 92.8%, $P < 0.001$; Fig. 3D; supplementary text section 2.3). To put these accuracy values into a biological context, we evaluated how many neurons would be necessary to achieve equal performance of the ER network with 200 neurons (Fig. 3D). In our simulations, a rodent-like network with higher reciprocity would need 380 neurons (90% more), whereas a humanlike network with fewer cycles would only need 150 neurons (25% less). Overall, our analytical and simulation results suggest that the network principles observed in the human temporal cortical layer 2-3 could be tuned to provide an increased variability of network activity across multiple dimensions (Fig. 3D). This could enhance the ability of local cortical microcircuits to retain rich input features for a longer time (*33*) and provide more flexible representation of sequential inputs (*21*).

Discussion

We have identified a predominantly directed and acyclic network architecture within the excitatory microcircuit of the human L2-3 temporal cortex. Such architecture could facilitate a hierarchical flow of information within the cortical layer, supporting sequential activation of neurons (*34*) and complex synaptic events (*35*). As local connectivity is mainly mediated through basal dendrites, these principles could represent prerequisites for bottom-up computations (*9*). This would be at odds with the previously suggested small-world network properties of the cortical microcircuit (*26*). In the rodent cortex, strong and reciprocally connected neurons are consistent with low dimensionality of in vivo population dynamics (*22*, *27*), a frequent observation in large-scale neural recordings (*36*). Whereas the biased connectivity along the dendrite-axon axis could represent a shared principle for introducing cost-efficient local directionality across species (*5*), the human L2-3 temporal cortex exhibits a more directed network topology owing to its random reciprocity and lack of cycles (*4*, *25*). Another aspect that differentiates the human cortex from the rodent cortex is the independence of synaptic strength and connectivity (*27*).

Limitations of our study include sampling of neurons within intersomatic distances of approximately 200 μm in the supragranular layer of the temporal cortex; recurrent connections at larger lateral distances or in other cortical layers and regions cannot be excluded. Cutting of axons during the slicing process is unavoidable. We minimized the impact of slice cutting on our results by morphological curation and additional analyses (fig. S2, C to E). The major limitation of studies based on resected cortical tissue is the lack of healthy control tissue. Consistent with previous studies on human resection tissue, which reported no differences in cellular or synaptic physiology regarding disease (*11*, *13*), our analysis indicated no significant effect of clinical epilepsy parameters on our results (fig. S6).

Finally, we show analytically and through simulations that each of the identified network principles can increase the network state space volume, which would allow higher dimensional representations of the local neuronal activity. Whereas this activity will further be constrained by interlaminar and long-range connectivity, such an increased dimensionality could allow information processing at longer timescales to retain and process complex inputs (*37*). To what extent these properties underlie the unique cognitive abilities of humans or represent a more general principle beyond the human temporal L2-3 cortex remains to be determined. Our results not only provide evidence for the implementation of directed acyclic graph–like topology in the human cortex but also could further serve as an inspiration for artificial neural network architectures.

REFERENCES AND NOTES

1. S. Recanatesi, G. K. Ocker, M. A. Buice, E. Shea-Brown, *PLOS Comput. Biol.* **15**, e1006446 (2019).
2. H. Ju, D. S. Bassett, *Nat. Neurosci.* **23**, 908–917 (2020).
3. H. Ko *et al*., *Nature* **473**, 87–91 (2011).
4. S. Song, P. J. Sjöström, M. Reigl, S. Nelson, D. B. Chklovskii, *PLOS Biol.* **3**, e68 (2005).
5. R. Perin, T. K. Berger, H. Markram, *Proc. Natl. Acad. Sci. U.S.A.* **108**, 5419–5424 (2011).
6. S. Rieubland, A. Roth, M. Häusser, *Neuron* **81**, 913–929 (2014).
7. S. J. Guzman, A. Schlögl, M. Frotscher, P. Jonas, *Science* **353**, 1117–1123 (2016).
8. Y. Peng *et al*., *Sci. Adv.* **7**, eabg4693 (2021).
9. K. D. Harris, G. M. Shepherd, *Nat. Neurosci.* **18**, 170–181 (2015).
10. R. D. Hodge *et al*., *Nature* **573**, 61–68 (2019).
11. J. Berg *et al*., *Nature* **598**, 151–158 (2021).
12. S. C. Seeman *et al*., *eLife* **7**, e37349 (2018).
13. L. Campagnola *et al*., *Science* **375**, eabj5861 (2022).
14. S. Hunt *et al*., *Cereb. Cortex* **33**, 2857–2878 (2023).
15. H. Planert *et al*., bioRxiv 2021.11.08.467668 [Preprint] (2023); https://doi.org/10.1101/2021.11.08.467668.
16. S. Loomba *et al*., *Science* **377**, eabo0924 (2022).
17. A. Gidon *et al*., *Science* **367**, 83–87 (2020).
18. L. Beaulieu-Laroche *et al*., *Cell* **175**, 643–651.e14 (2018).
19. R. Fang *et al*., *Science* **377**, 56–62 (2022).
20. E. R. E. Schmidt *et al*., *Nature* **599**, 640–644 (2021).
21. S. Bernardi *et al*., *Cell* **183**, 954–967.e21 (2020).
22. D. Dahmen *et al*., bioRxiv 2020.11.02.365072 [Preprint] (2022); https://doi.org/10.1101/2020.11.02.365072.
23. Y. Peng *et al*., *eLife* **8**, e48178 (2019).
24. S. Lefort, C. Tomm, J.-C. Floyd Sarria, C. C. H. Petersen, *Neuron* **61**, 301–316 (2009).
25. N. L. Turner *et al*., *Cell* **185**, 1082–1100.e24 (2022).
26. E. Gal *et al*., *Nat. Neurosci.* **20**, 1004–1013 (2017).
27. L. Cossell *et al*., *Nature* **518**, 399–403 (2015).
28. R. Milo *et al*., *Science* **298**, 824–827 (2002).
29. M. Vegué, R. Perin, A. Roxin, *J. Neurosci.* **37**, 8498–8510 (2017).
30. E. Gal, R. Perin, H. Markram, M. London, I. Segev, bioRxiv 656058 [Preprint] (2020); https://doi.org/10.1101/656058.
31. M. W. Reimann *et al*., *Front. Comput. Neurosci.* **11**, 48 (2017).
32. J. Wilting, V. Priesemann, *Curr. Opin. Neurobiol.* **58**, 105–111 (2019).
33. P. V. Aceituno, G. Yan, Y.-Y. Liu, *iScience* **23**, 101440 (2020).
34. Y. Ikegaya *et al*., *Science* **304**, 559–564 (2004).
35. G. Molnár *et al*., *PLOS Biol.* **6**, e222 (2008).
36. C. Stringer *et al*., *Science* **364**, eaav7893 (2019).
37. M. S. Goldman, *Neuron* **61**, 621–634 (2009).
38. Y. Peng *et al*., Data from: Directed and acyclic synaptic connectivity in the human layer 2-3 cortical microcircuit, Dryad (2024); https://doi.org/10.5061/dryad.t76hdr87b.

ACKNOWLEDGMENTS

We thank V. Lopes dos Santos for comments on a previous version of the manuscript. We thank A. Wilke and D. Do Minh for technical support. **Funding:** This work was supported by the

German Research Foundation (DFG) under Germany's Excellence Strategy (EXC-2049-390688087 to D.S.); DFG Walter Benjamin Fellowship (451242556 to Y.P.); DFG Retune TRR 295 (424778381 to J.R.P.G.); Swiss National Science Foundation (CRSII5-173721 and 315230\189251 to B.F.G.); ETH project funding (ETH-20 19-01 to B.F.G.); the Human Frontier Science Program (RGY0072/2019 to B.F.G.); and ETH Zurich Postdoc fellowship to P.V.A. **Author contributions:** Conceptualization: J.R.P.G., Y.P., and A.B. Graph analysis and random models: A.B. and Y.P. Neural network simulations and analysis: P.V.A. Data acquisition: Y.P., F.X.M., and H.P. Anatomical reconstruction: S.G. and I.V. Patient material: P.F., J.O., M.H., K.F., T.K., and M.S. Neuropathological assessment: H.R. Funding acquisition and resources: J.R.P.G., Y.P., D.S., P.V.A., and B.F.G. Supervision: J.R.P.G. and B.F.G. Writing – original draft: Y.P., J.R.P.G., A.B., and P.V.A. Writing – review & editing: Y.P., A.B., P.V.A., H.A., F.X.M., H.P., B.F.G., and J.R.P.G. **Competing interests:** M.H. reports consultancy within the past 3 years for Angelini, Bial, Desitin, Eisai, German Medical Association Medicines Commission, Jazz Pharma, Nutricia, the Federal Joint Committee, and UCB. **Data and materials availability:** The processed data and code used to generate the results, simulations, and visualizations are available in Dryad (*38*). Resected human brain tissues from Bielefeld were made available under a material transfer agreement between Evangelisches Klinikum Bethel gGmbH (Bielefeld) and Charité–Universitätsmedizin Berlin.

SUPPLEMENTARY MATERIALS

science.org/doi/10.1126/science.adg8828
Materials and Methods
Supplementary Text
Figs. S1 to S12
References (*39*–*74*)
MDAR Reproducibility Checklist

Submitted 27 January 2023; resubmitted 9 October 2023
Accepted 12 March 2024
10.1126/science.adg8828